Physical characteristics and infrared fluorescence properties of sol–gel derived Er 3+ – Yb 3+ codoped TiO 2

Chu-Chi Ting, San-Yuan Chen, and Hsin-Yi Lee

Citation: Journal of Applied Physics **94**, 2102 (2003); doi: 10.1063/1.1590411
View online: http://dx.doi.org/10.1063/1.1590411
View Table of Contents: http://scitation.aip.org/content/aip/journal/jap/94/3?ver=pdfcov
Published by the AIP Publishing

Physical characteristics and infrared fluorescence properties of sol–gel derived $Er^{3+}-Yb^{3+}$ codoped TiO_2

Chu-Chi Ting and San-Yuan Chen
Department of Materials Science and Engineering, National Chiao-Tung University, Hsinchu, Taiwan 300, Republic of China

Hsin-Yi Lee[a)]
Research Division, National Synchrotron Radiation Research Center, Hsinchu, Taiwan 30077, Republic of China

(Received 21 February 2003; accepted 19 May 2003)

$Er^{3+}-Yb^{3+}$ codoped TiO_2 films were prepared on fused silica by sol–gel processes. The Yb^{3+} codoping effect on the physical characteristics and ~1.54 μm photoluminescence (PL) properties of Er^{3+}-doped TiO_2 films was investigated. Maximum ~1.54 μm PL intensity occurs in Er^{3+} (5 mol %)–Yb^{3+}(30 mol %) codoped TiO_2 samples annealed at 700 °C. However, when the concentration of Yb^{3+} ions is more than 30 mol %, the back energy transfer effect from Er^{3+} to Yb^{3+} will deteriorate the ~1.54 μm PL efficiency. Extended x-ray absorption fine structure measurements show that the average spatial distance between Er^{3+} ions is slightly decreased due to the partial substitution of Yb^{3+} for Er^{3+} ions in the local structure. The Yb^{3+} ion in the $Er^{3+}-Yb^{3+}$ codoped TiO_2 samples not only plays the role of disperser but is also a sensitizer of the Er^{3+} ion. This dual effect leads to larger PL intensity in the $Er^{3+}-Yb^{3+}$ codoped TiO_2 system in comparison with $Er^{3+}-Y^{3+}$ codoped TiO_2 samples. Compared with SiO_2 films with Er^{3+} (5 mol %)–Yb^{3+} (30 mol %) codoped and annealed at optimal temperature of 985 °C, the $Er^{3+}-Yb^{3+}$ codoped TiO_2 film obtains better PL properties at lower annealing temperature.
[DOI: 10.1063/1.1590411]

I. INTRODUCTION

Erbium-doped materials can act as an optical gain medium in optical communication systems because the optical transition of Er^{3+} ions occurs at an eye-safe wavelength of ~1.54 μm which coincides with the third maximum transparent window of silica-based optical fibers.[1–3] In order to achieve high gain optical amplification in compact optoelectronic devices, a high doping concentration of Er^{3+} ions is required. However, emission efficiency of ~1.54 μm photoluminescence (PL) will be degraded for higher concentration Er^{3+}-doped fiber amplifiers because of the concentration quenching effect.[4,5] Codopants of Al^{3+}, Y^{3+}, and Yb^{3+} are usually adopted to inhibit Er^{3+} clustering and to promote a more uniform spatial distribution of Er^{3+} ions in Er-doped silica.[6–8]

TiO_2 film has higher refraction index ($n=2.52$ for anatase and $n=2.76$ for rutile) as well as lower phonon energy (<700 cm^{-1})[9] than silica glass film. Recently, it has been demonstrated that Er^{3+}-doped TiO_2-based films show potential for application in microintegrated photonic devices. There are some advantages of a TiO_2 thin film optical waveguide. For instance, it has high transparency in the visible to the near-infrared wavelength regions. The high refractive index ($n=2.75$ and 2.54 at $\lambda=550$ nm for rutile and anatase phases, respectively) allows the use of small waveguide bending radii (<100 μm), which leads to a reduction in device dimensions. In addition, when a TiO_2 planar waveguide is cladded with SiO_2 ($n=1.45$), the high contrast in refractive index between the core and cladding layers can result in high confinement of the optical mode in the guide. However, few detailed studies have been made to investigate the role of rare-earth codopants for the PL properties of Er^{3+}-doped TiO_2 films.[10,11] In a previous report, we demonstrated that the ~1.54 μm PL properties can be enhanced by a factor of 10 in intensity and 1.5 times for the full width at half maximum (FWHM) in $Er^{3+}-Y^{3+}$ codoped TiO_2 films in comparison with the $Er^{3+}-Al^{3+}$ codoped SiO_2 system.[12] The enhanced PL emission of $Er^{3+}-Y^{3+}$ codoped TiO_2 films is attributed to sufficient dispersion and the distortion of the local structure of Er^{3+} ions in the TiO_2 host matrix by yttrium codoping.

On the other hand, a Yb^{3+} codopant has been demonstrated as increasing variation of the Er sites which results in the inhomogeneous broadening effect.[13] In addition, a Yb^{3+} ion can sensitize Er^{3+} ions and enhance the ~1.54 μm PL intensity.[14] This mechanism makes the population of the $^4I_{11/2}$ Er^{3+} level increase and leads to enhancement of the ~1.54 μm PL efficiency. Gu *et al.* studied Er^{3+} and Yb^{3+} ion codoped silica thin films prepared by rf magnetron sputtering and reported that the enhanced PL intensity is a result of the transfer of energy from Yb^{3+} to Er^{3+}.[15] However, the role of the Yb^{3+} ion in phase development and in optical properties related to the Er^{3+}-doped TiO_2 system has not been investigated. Therefore, it is very important to investigate the influence of codopant Yb^{3+} on the physical charac-

[a)]Author to whom correspondence should be addressed; electronic mail: hylee@srrc.gov.tw

teristics and optical properties of Er^{3+}-doped titania.

Although $Yb^{3+}/Y^{3+}/Er^{3+}$ ions have similar ionic radii ($Yb^{3+}=0.0862$, $Y^{3+}=0.0892$, and $Er^{3+}=0.0881$ nm)[16] and $Yb_2O_3/Y_2O_3/Er_2O_3$ has nearly the same crystal structure and lattice constant, Yb^{3+} and Y^{3+} belong to different chemical groups. Yb is characteristic of intra-$4f$ transition and the outer closed $5s^25p^6$ shells screen the unfilled inner $4f$ (Ref. 11) shell but Y does not have an intra-$4f$ transition orbital.[17,18]

Therefore, in this work, the role of Yb^{3+} and Y^{3+} codopants for the photoluminescence properties of Er^{3+}-doped titania materials will be studied. A further comparison of $\sim$1.54 μm PL is made to clarify the role of Yb^{3+} and Y^{3+} codopants in Er^{3+}-doped TiO_2 based on structural similarity and different characteristics between Yb^{3+} and Y^{3+} ions.

II. EXPERIMENTAL PROCEDURE

A. Sample preparation

Acetic acid (HAc) (Merck) and 2-methoxyethanol (MOE) (Merck) with molar ratio of Ti/HAc/MOE=1/10/15 were first added to titanium isopropoxide (Alfa), followed by stirring for 30 min. Subsequently, the ytterbium acetate (Alfa) and erbium acetate (Alfa) powders were dissolved in the titanium solution and stirred for 10 h to create a homogeneous hydrolysis/polymerization reaction. The molar ratios of Er^{3+}/Ti^{4+} and Yb^{3+}/Ti^{4+} were varied from 0.5 to 10 and 10 to 50 mol %, respectively.

For thin-film fabrication, the $Er^{3+}-Yb^{3+}$ codoped TiO_2 precursor solution was spin coated onto fused silica substrates (2×2 cm^2). The as-deposited sol–gel films were first pyrolyzed under dry oxygen atmosphere at 400 °C for 30 min at a heating rate of 3 °C/min and then annealed at temperatures ranging from 600 to 1000 °C for 1 h in dry oxygen atmosphere. Multiple spin-coating processes were employed to deposit 0.5 ± 0.02 μm thick films for each sample with different $Er^{3+}/Yb^{3+}/Ti^{4+}$ molar ratios. Moreover, each sample was prepared for five species carefully fabricated under the same conditions for further measurement of the fluorescence intensity. For comparison, $Er^{3+}-Y^{3+}$ codoped TiO_2 films prepared using the same procedure were also fabricated.[12]

B. Characterization measurements

The crystal structure of samples was analyzed by a Mac Science 18 kW x-ray diffractometer with Cu $K\alpha$ radiation at the in-house x-ray laboratory at the National Synchrotron Radiation Research Center (NSRRC), Hsinchu, Taiwan. Erbium L_{III}-edge x-ray absorption spectra were recorded at the BL17C wiggler beamline at NSRRC. The electron storage ring was operated at energy of 1.5 GeV and a current of 120–200 mA. A Si (111) double-crystal monochromator with a 0.5 mm entrance slit was used for energy scanning. The energy resolution, $\Delta E/E$, was about 1.9×10^{-4}. Measurements were performed at room temperature in fluorescence mode and the sample was positioned 45° to the incident x-ray beam. The pre-edge background of x-ray absorption spectra, which was fit to a straight line, was extrapolated throughout the entire range of data and then subtracted. The postedge background was simulated by a cubic spline in order to isolate extended x-ray absorption fine structure (EXAFS) oscillations from the overall absorption. The EXAFS function, so-called $\chi(k)$ data, was obtained by subtracting the postedge background from the overall absorption data followed by normalization to the edge step. After being weighted by k^3, where k is the photoelectron wave vector, the χ data in the range of $2.75<k<11.25$ Å^{-1} were Fourier transformed into r space. The data in r space between 0 and 10 Å were then windowed and backtransformed (filtered) to get rid of high-frequency noise for subsequent comparison. Polycrystalline Er_2O_3 powder (Cerac, 99.9%) was used as a reference standard.

Fourier transform infrared (FTIR) spectra were recorded on a Perkin-Elmer 580 spectrometer. A 980 nm diode laser with power of 50 mW was used as the pump source inclined 45° to irradiate the center of the samples and the fluorescence spectra were recorded normal from the samples at room temperature using a spectrophotometer equipped with a liquid N_2-cooled Ge detector to detect infrared fluorescence. In order to compare the fluorescence intensity of different samples, the distance and position between the samples and spectrophotometer were fixed exactly for each measurement, and the fluorescence intensity of each sample was the average value of five species.

III. RESULTS AND DISCUSSION

A. Structural evolution

Typical x-ray diffraction (XRD) was used to investigate the effect of the annealing temperature on the structural development of Er^{3+} (5 mol %)-doped TiO_2. As shown in Fig. 1(a), at 700 °C, both anatase and rutile phases formed. As the sample was annealed at 800 °C, a weak XRD peak corresponding to $Er_2Ti_2O_7$ pyrochlore phase (P) was detected. However, for the Er^{3+} (5 mol %)$-TiO_2$ with Yb^{3+} (30 mol %) codoped, the XRD patterns in Fig. 1(b) show that at 700 °C, the host matrix becomes amorphous in contrast to that [Fig. 1(a)] of the sample without Yb^{3+} codopant. It is obvious that the addition of more than 30 mol % Yb^{3+} ions can lead to destruction of the TiO_2 network structure. The grain size of the Er^{3+} (5 mol %)-doped TiO_2 sample annealed at 700 °C is estimated, according to the Scherrer formula,[19] to be approximately 60 Å, while the grain size of 900 and 1000 °C annealed film is $\sim$390 and $\sim$500 Å, respectively. However, the Er^{3+} (5 mol %)$-TiO_2$ with Yb^{3+} (30 mol %) codoped film annealed at 700 °C shows an amorphous matrix while grains of 900 and 1000 °C annealed film are $\sim$240 and $\sim$390 Å, respectively. Therefore, the grain size can be made smaller by adding doping Yb^{3+} to the system. This is beneficial for the application of waveguides because smaller grain size can reduce light scattering. Furthermore, at 800 °C, it was found that the pyrochlore phase has fully developed. After the $Er^{3+}-Yb^{3+}$ codoped TiO_2 samples were annealed at 900–1000 °C, both the rutile (R) and pyrochlore

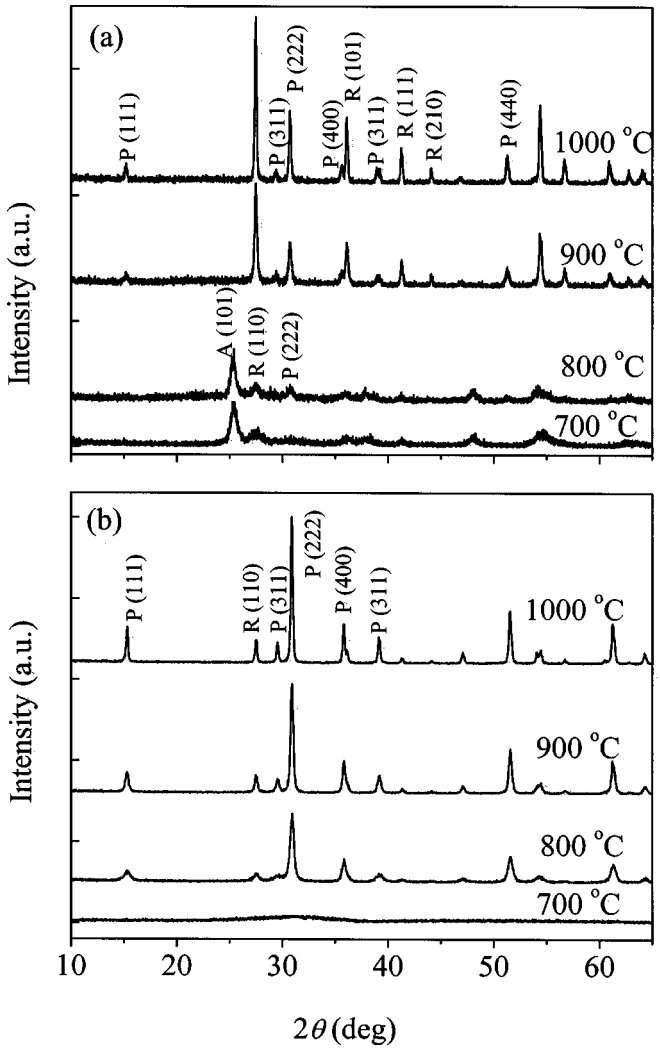

FIG. 1. X-ray diffraction patterns of (a) Er^{3+} (5 mol %)-doped TiO_2 and (b) with 30 mol % Yb^{3+} codopant annealed from 700 to 1000 °C for 1 h.

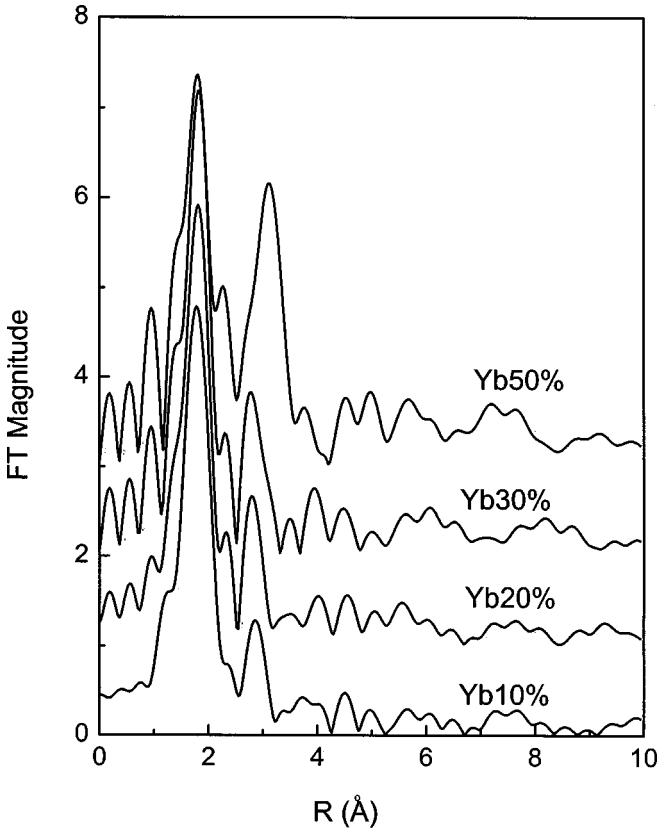

FIG. 2. Fourier transform of the EXAFS function at the Er L_{III} edge for Er^{3+} (5 mol %)-doped TiO_2 samples with 0–50 mol % Yb^{3+} codopant annealed at 700 °C for 1 h.

(*P*) phases become well crystallized. Similar results are also observed in the $Y^{3+}-Er^{3+}$ codoped TiO_2 system (not shown here).

Figure 2 shows pseudoradial distribution functions obtained from k^3-weighted Fourier transforms of the $Er^{3+}-Yb^{3+}$ codoped TiO_2 samples annealed at 700 °C for 1 h. The local structural parameters, such as the interatomic distance, coordination number, and Debye–Waller factor (a measure of disorder of neighboring atoms around an absorbing atom) can be extracted from the EXAFS function. However, no attempt was made to perform a detailed analysis in this work. Instead, a qualitative comparison will be presented here. From the Fourier transform of the EXAFS function shown in Fig. 2, the first shell bond distance around Er^{3+} is ~1.81 Å which is close to the Er–O bond length (~1.86 Å) of a standard Er_2O_3 sample. (According to theoretical calculation of a standard Er_2O_3 sample, it was found that the shift in phase makes the pseudoradial distance approximately 0.46 Å shorter than the real distance in this measurement.) Qualitative observation of the 700 °C-annealed samples (i.e., no formation of pyrochlore phase) reveals that its EXAFS functions are not significantly different for concentration of $Yb^{3+} \leqslant 30\%$. This indicates that the local structure around Er^{3+} ions in $Er^{3+}-Yb^{3+}$ codoped TiO_2 systems is similar for those samples. Additionally, it is noted that the second-neighbor distance around Er^{3+} slightly decreased from 2.855 to 2.775 Å when the concentration of Yb^{3+} increased from 10 to 30 mol %. The shorter second shell distance is proof that Yb ions may replace the second shell position of Er–O–Er. In other words, Er–O–Er–O–Er is partially replaced by Er–O–Yb–O–Er. This phenomenon can be attributed to the fact that since Er^{3+} and Yb^{3+} have the same valence and are close in ionic radii, they can be replaced with each other. However, as the Er^{3+}-doped TiO_2 was codoped with 50 mol % Yb^{3+}, the second-neighbor distance around Er^{3+} became larger compared to that with 30 mol % Yb^{3+} codoped which is probably due to high disorder around Er^{3+} ions or the formation of clusters.

For the sample annealed at (800 or 900 °C), the well crystallized pyrochlore crystallites were generated within the TiO_2 host matrix. EXAFS analysis in Fig. 3 shows that the Er sites have very different local environments compared with those of samples without pyrochlore crystallites. These titanate-pyrochlore phases have a general formula, $A_2B_2O_7$, in which the *A* site can be rare-earth (Ln) and the *B* site titanium (3*d* transition element). It is interesting to note that $Er_2Ti_2O_7$ and $Yb_2Ti_2O_7$ pyrochlore phases have the same lattice structure and similar lattice constants. Therefore, the pyrochlore phases in $Er^{3+}-Yb^{3+}$ codoped TiO_2 samples are structurally indistinguishable. In addition, $Yb_2Ti_2O_7$ pyro-

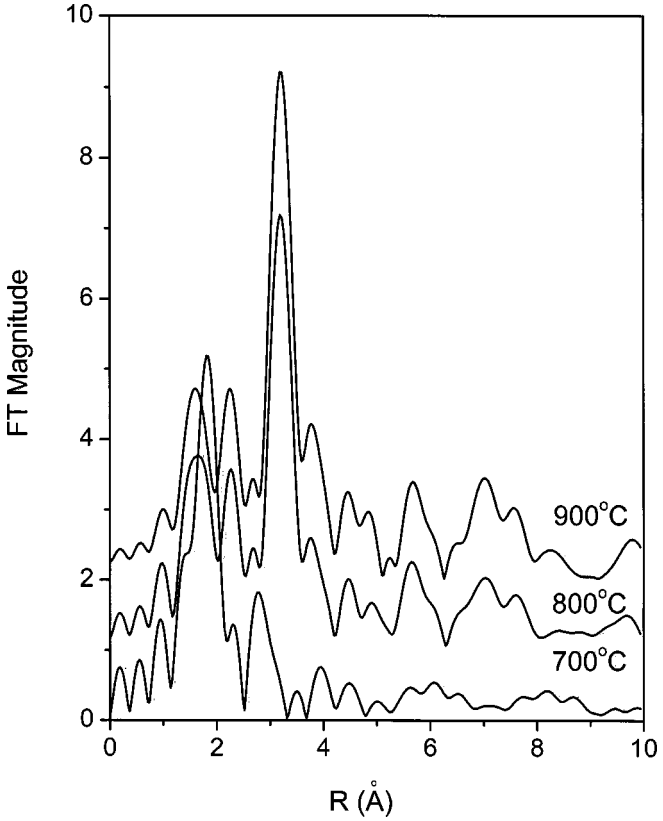

FIG. 3. Fourier transform of the EXAFS function at the Er L_{III} edge for Er^{3+} (5 mol %)$-Yb^{3+}$ (30 mol %) codoped TiO_2 samples annealed at various temperatures for 1 h.

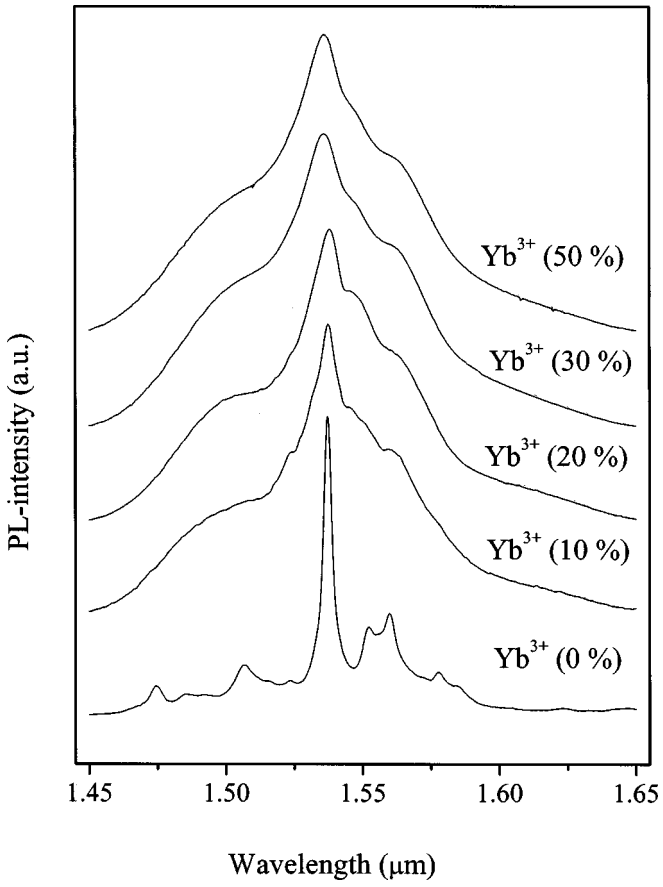

FIG. 4. ~1.54 μm PL spectra of Er^{3+} (5 mol %)-doped TiO_2 samples with 0–50 mol % Yb^{3+} codopant annealed at 700 °C for 1 h. All the spectra were normalized to the same intensity to compare the differences in spectral feature.

chlore phase with a smaller cation exhibits smaller a lattice constant (i.e., smaller distance between $A-A$ cations). In the pyrochlore phase, Ti^{4+} ions are sixfold coordinated and located within trigonal antiprisms with all six anions equal distances from the center Ti^{4+} cations. However, Er^{3+} (Yb^{3+}) ions are eightfold coordinated and located within scalenohedra (distorted cubes) that contain six equal space anions at a slightly shorter distance from the center Er^{3+} (Yb^{3+}) cations.[20] The aforementioned local structural evolution of Er^{3+} ions can considerably influence the photoluminescence properties of $Er^{3+}-Yb^{3+}$ (or $Er^{3+}-Y^{3+}$) codoped TiO_2 systems.

B. ~1.54 μm photoluminescence properties

Figure 4 shows ~1.54 μm PL spectra of the Er^{3+} (5 mol %)-doped TiO_2 samples with 0–50 mol % Yb^{3+} added annealed at 700 °C for 1 h. All of the spectra were normalized to the same intensity to compare differences between spectral features. The Er^{3+} (5 mol %)-doped TiO_2 sample exhibits a sharp PL spectrum with a 1.537 μm main peak which is characteristic of Er^{3+} emission ($^4I_{13/2}\rightarrow{}^4I_{15/2}$). However, by increasing the Yb^{3+} codopant concentration, the PL spectra become broader. The maximum bandwidth (FWHM = 67 nm) of ~1.54 μm PL spectra was obtained for the sample with added Yb^{3+} content above 30 mol %. The line-broadening mechanism can be attributed to the inhomogeneously broadened transition of Er^{3+} ions.[21] For the sample without Yb^{3+} codopant, the well-resolved spectrum demonstrates that the Er^{3+} ions are located in well-defined sites in the TiO_2 matrix. Namely, each Er^{3+} ion occupies a similar type of site that has well-defined surroundings and, hence, each Er^{3+} ion experiences similar crystal fields. However, the Yb^{3+} codopant can destroy the network of the TiO_2 host matrix, which results in varying Er sites with different surrounding environments and causes randomization of the Stark splittings. Therefore, the overall spectral lines that result from superimposed contributions of each Er site are inhomogeneously broadened.

Figure 5 illustrates that the influence of the annealing temperature on the ~1.54 μm PL spectral feature of Er^{3+} (5 mol %)$-Yb^{3+}$ (30 mol %) codoped TiO_2 samples. As the samples were annealed above 800 °C, the spectra with many split lines were detected. From the XRD patterns in Fig. 1(a), it is seen that $Er_2Yb_{2-x}Ti_2O_7$ crystallites were generated at annealing temperatures above 800 °C. This means that the majority of Er^{3+} ions should be located in the crystalline $Er_2Yb_{2-x}Ti_2O_7$ phase and that the Er^{3+} bonding environment becomes uniform and produces the well-resolved PL spectrum. For comparison, an Er^{3+} (5 mol %)$-Yb^{3+}$ (30 mol %) codoped silica film was also prepared and annealed at optimal temperature of ~985 °C.[22] Figure 6 illustrates that the PL properties of the $Er^{3+}-Yb^{3+}$ codoped TiO_2 system exhibit more intense emission (~ two times more) and a

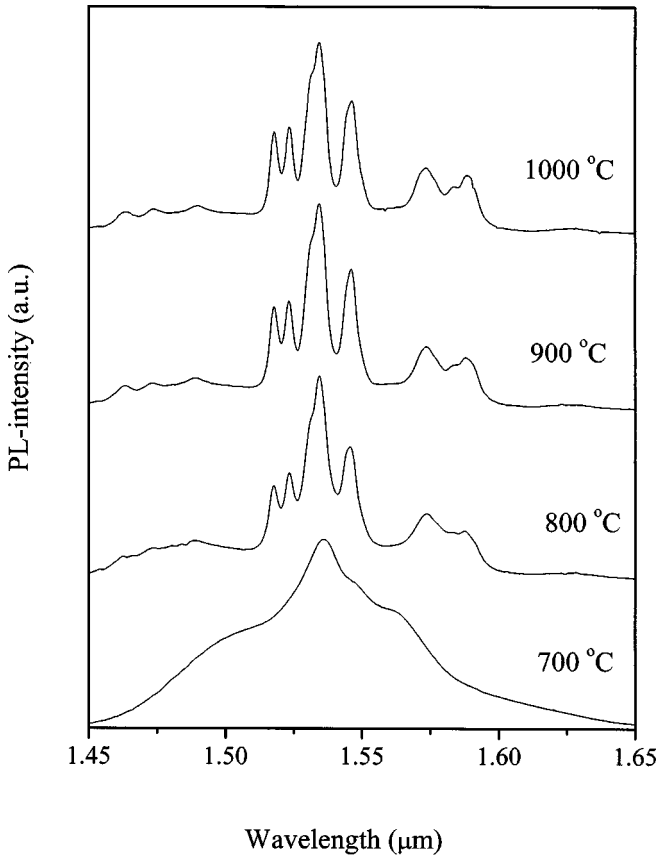

FIG. 5. ~1.54 μm PL spectra of Er^{3+} (5 mol %)–Yb^{3+} (30 mol %) codoped TiO_2 annealed from 700 to 1000 °C for 1 h. All the spectra were normalized to the same intensity to compare the differences in spectral features.

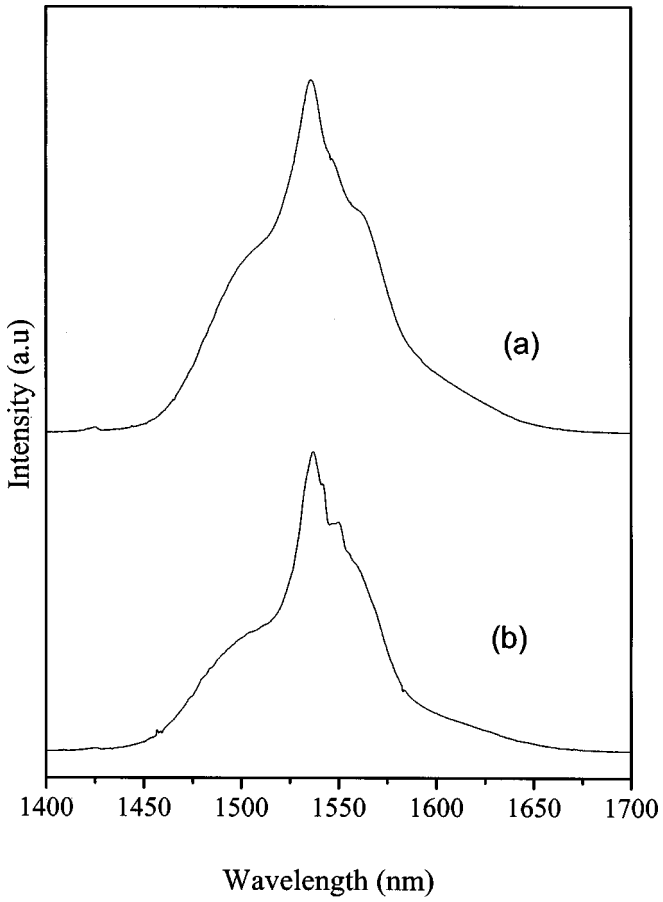

FIG. 6. Comparison of ~1.54 μm PL spectra of (a) Er^{3+}–Yb^{3+} codoped TiO_2 and (b) Er^{3+}–Yb^{3+} codoped SiO_2 annealed at optimal temperatures of 700 and 985 °C for 1 h, respectively.

wider FWHM (~1.5 times more) than those of an optimal Er^{3+}–Yb^{3+} codoped SiO_2 system. This implies that the PL properties strongly depend on the composition and structure of the host materials. Furthermore, the Er^{3+}–Yb^{3+} codoped TiO_2 film not only obtains better PL properties but also a lower annealing temperature.

The dependence of the annealing temperature on the PL intensities of Er^{3+} (5 mol %)–Yb^{3+} (30 mol %) codoped TiO_2 samples is shown in Fig. 7. The final PL intensity seen often results from the competition between the content of hydroxyl groups (i.e., quenching centers) and the symmetry of local structure around the Er^{3+} ions. The increase in PL intensity from 600 to 700 °C is attributed to the reduction of the OH^- hydroxyl content as one can see in Fig. 8. The FTIR absorption around 4000–3000 cm^{-1}, corresponding to O–H vibration mode, decreases with an increase of the annealing temperature.[23–25] However, above 800 °C, the PL intensity is abruptly reduced and this is strongly related to the formation of $Er_xYb_{2-x}Ti_2O_7$ pyrochlore phase as evidenced from XRD patterns in Fig. 1(b). The local structure around Er^{3+} ions in well-crystallized $Er_xYb_{2-x}Ti_2O_7$ phase (above 800 °C) becomes more symmetric compared to that of Er^{3+} ions in the amorphous host matrix (700 °C) and may result in less probability of the normally forbidden intra-4f transition of Er^{3+} ions and degradation of the PL efficiency.[26–28] Similar temperature dependence of Er–Yb codoped TiO_2 on the PL intensity is also observed in the Er–Y codoped TiO_2 system.

The variation of the ~1.54 μm PL intensity of Er^{3+}–Yb^{3+} codoped TiO_2 samples with the Er^{3+}–Yb^{3+} concentration is summarized in Fig. 9. When the Yb^{3+} codoping concentration is 10 mol %, the variation of PL intensity shows the phenomenon $I_{(1\%)}>I_{(5\%)}>I_{(10\%)}$ (where $I_{(1\%)}$ represents the PL intensity of the sample with 1 mol % Er^{3+} doping dose). However, for Yb^{3+} codoping concentration above 10 mol %, the phenomenon changes to $I_{(5\%)}>I_{(10\%)}>I_{(1\%)}$. This indicates that 10 mol % Yb^{3+} codoping concentration is still not enough to disperse Er^{3+} ions very well and a large number of Er^{3+} ions (5 and 10 mol %) can still form clusters. When 20 mol % Yb^{3+} codoping concentration was used, however, the influence of concentration quenching on $I_{(5\%)}$ and $I_{(10\%)}$ can be considerably reduced.

For the sample with Yb^{3+} concentration above 30 mol %, as the poorly crystalline pyrosilicate phase ($Er_xYb_{2-x}Ti_2O_7$) crystallized in the host matrix, it can be assumed that the Er^{3+} ions are located in the $Yb_2Ti_2O_7$ matrix. If the Er^{3+} ions were postulated to randomly disperse in $Er_xYb_{2-x}Ti_2O_7$ phases, then the average spatial distance between Er^{3+} ions would be enlarged because some Er sites were occupied by Yb^{3+} ions. The PL intensity can be remarkably enhanced by the reduction of Er–Er quenching effect and at this time, the Er–Yb energy transfer effect still

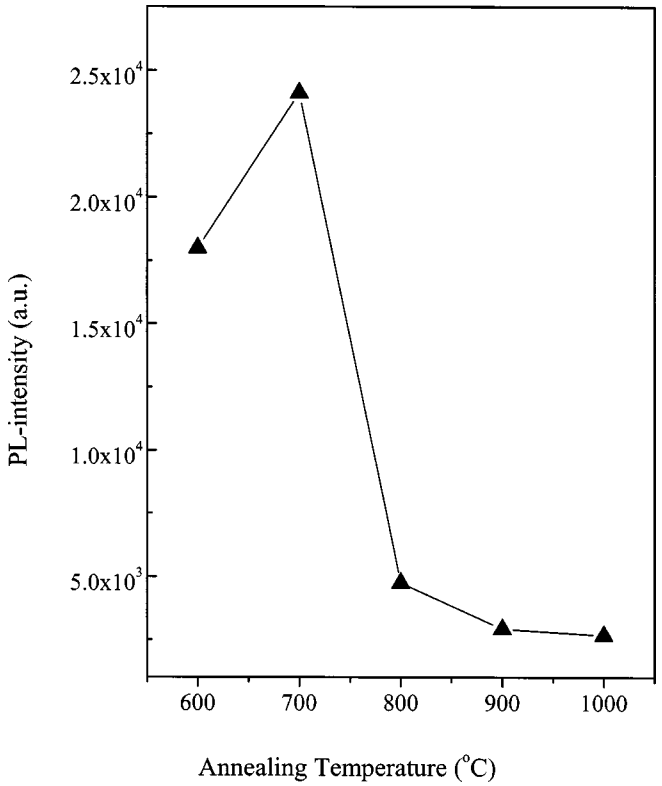

FIG. 7. PL intensity of Er^{3+} (5 mol %)-doped TiO_2 samples with 30 mol % Yb^{3+} codopant annealed from 600 to 1000 °C for 1 h.

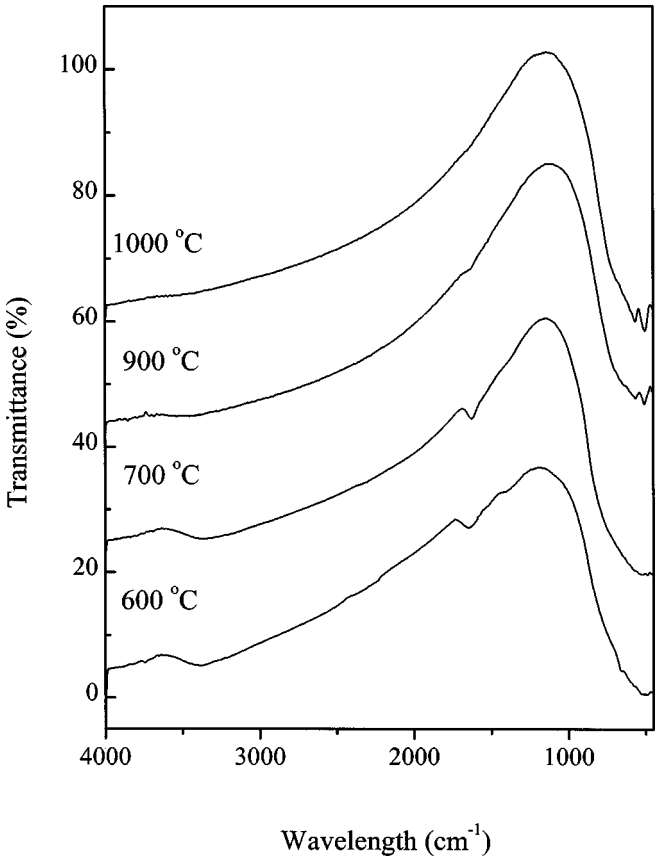

FIG. 8. FTIR transmittance spectra of Er^{3+} (5 mol %)–Yb^{3+} (30 mol %) codoped TiO_2 annealed from 600 to 1000 °C.

does not dominate. Nevertheless, the 50 mol % Yb^{3+} codopant leads to the reduction of PL intensities that might be related to the back energy transfer from Er^{3+} to Yb^{3+} ions (i.e., double energy transfer)[29] and resonant energy migration between Yb^{3+} ions.

For comparison, Er^{3+}(5 mol %)–Y^{3+}(10–50 mol %) codoped TiO_2 films were also prepared and annealed at the same annealing temperature of 700 °C. The ~1.54 μm PL spectra (not shown here) of the Er^{3+}–Y^{3+} codoped TiO_2 samples exhibit a similar phenomenon to that of the Er^{3+}–Yb^{3+} codoped TiO_2 samples. Enhancement of PL intensities with an increase in Y^{3+} content up to 50 mol % was observed for the Er^{3+} (5 mol %)–Y^{3+} (10–50 mol %) codoped TiO_2 samples, shown in Fig. 10. In contrast, maximum PL intensity appears in the sample of Er^{3+} (5 mol %)–Yb^{3+} (30 mol %) codoped TiO_2, above that, reduced PL intensity was observed, like in the sample with 50 mol % Yb^{3+}. The comparison of the PL intensities of the TiO_2 codoped with Er^{3+} (5 mol %)–Yb^{3+} (30 mol %) with the sample codoped with Er^{3+} (5 mol %)–Y^{3+} (30 mol %) demonstrates that the PL intensity in the former is about ~ two times higher than that in the latter. According to the aforementioned results, the mechanisms for the enhancement of PL intensity between Er–TiO_2 doped with Yb^{3+} and Y^{3+} are somewhat different.

Because Er^{3+} and Yb^{3+} (or Y^{3+}) have the same valence and similar ionic radii, they could be replaced by each other and the –Er–O–Er–O–Er– bonding structures can be changed into –Er–O–[Yb (or Y^{3+})–O]$_n$–Er–. Therefore, the more the Y^{3+} codopant the larger the atomic spacing among Er^{3+} ions and the enhanced PL properties that can be attributed to an increase in dispersion and solubility of Er^{3+} ions in Er^{3+}–Yb^{3+} (or Er^{3+}–Y^{3+}) codoped TiO_2 systems. However, it is worth noting that with an increase of Yb^{3+} up to 30 mol %, the PL intensity was remarkably enhanced. This implies that the Yb^{3+} ion not only plays the role of disperser but also that of sensitizer for Er^{3+} ions. This dual effect might have superimposed impact on the ~1.54 μm PL efficiency, which seems consistent with our experimental results that Er^{3+}–Yb^{3+} (10–30 mol %) codoped TiO_2 samples have larger PL intensity than Er^{3+}–Y^{3+} (10–30 mol %) codoped TiO_2 samples.

However, for Yb^{3+} concentration greater than 30 mol %, the ~1.54 μm PL efficiency was reduced and that can be attributed to two deleterious processes:[29–31] (i) back energy transfer from Er^{3+} to Yb^{3+} ions and (ii) double energy transfer (DET) where a second excited Yb^{3+} ion transfers its energy to the excited Er^{3+} ion, which results in promoting the Er^{3+} energy level from the $^4I_{11/2}$ to the $^4F_{7/2}$ manifold. On the other hand, although Y^{3+} also possesses similar valence and ionic radius as Er^{3+}, DET does not show up in the Er^{3+}–Y^{3+} codoped TiO_2 system because Y^{3+} is not an optically active element. Therefore, with an increase in Y^{3+} concentration, the PL intensity continuously increased and that can be attributed to an increase in dispersion and distortion of the local structure of Er^{3+} ions in Er^{3+}–Y^{3+} codoped TiO_2 films.

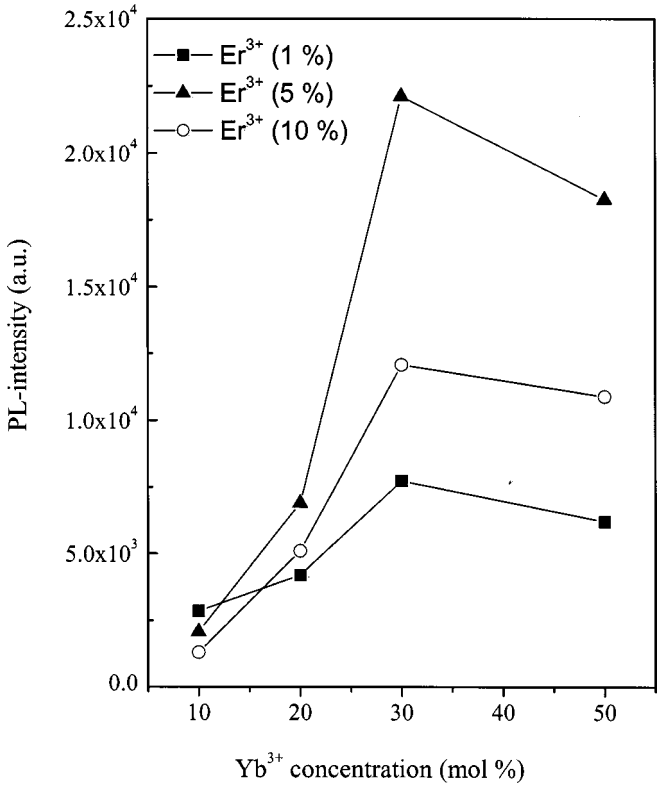

FIG. 9. Dependence of the Yb^{3+} concentration on the ~1.54 μm PL intensity of $Er^{3+}-Yb^{3+}$ codoped TiO_2 samples with different concentration Er^{3+} ions added annealed at 700 °C for 1 h.

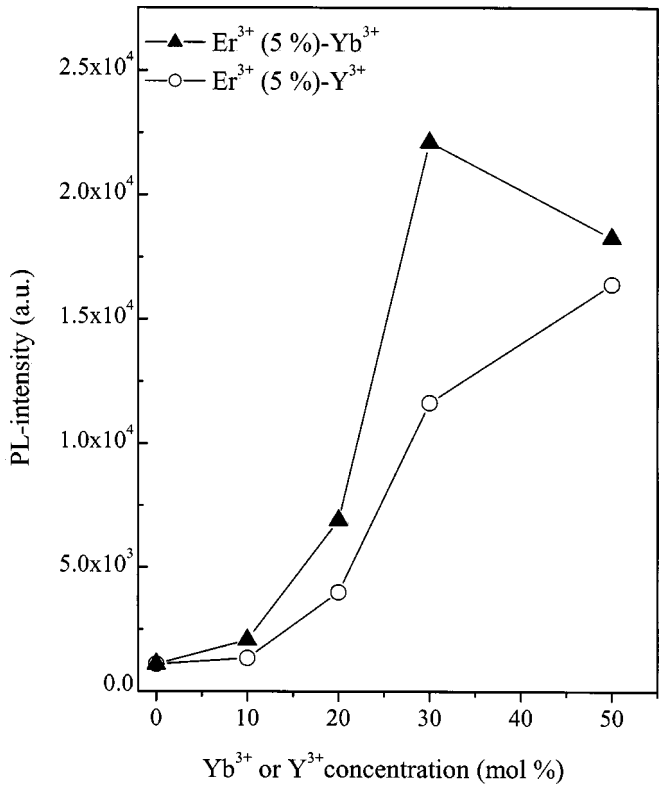

FIG. 10. Comparison of ~1.54 μm PL intensities between Er^{3+} (5 mol %)$-Yb^{3+}$ (10–50 mol %) and Er^{3+} (5 mol %)$-Y^{3+}$ (10–50 mol %) codoped TiO_2 systems annealed at 700 °C for 1 h.

IV. CONCLUSIONS

Maximum ~1.54 μm PL intensity was obtained for the Er^{3+} (5 mol %)$-Yb^{3+}$ (30 mol %) codoped TiO_2 sample annealed at 700 °C. This can be attributed to the competition between the content of hydroxyl groups and the Er site symmetry. Below 700 °C, the content of hydroxyl groups plays an important role in the PL intensity. On the other hand, above 700 °C, the pyrochlore phases that form in the $Er^{3+}-Yb^{3+}$ codoped TiO_2 systems can result in degradation of the ~1.54 μm PL efficiency and the formation of well-resolved spectral lines. The average spatial distance between Er^{3+} ions in $Er^{3+}-Yb^{3+}$ codoped TiO_2 films slightly decreased due to partial substitution of Yb^{3+} for Er^{3+} ions in the local structure. This indicates that the Yb^{3+} ion can act as a disperser of Er^{3+} ions and reduce the concentration quenching effect. Therefore, in comparison with the $Er^{3+}-Y^{3+}$ codoped TiO_2 samples, the Yb^{3+} ion in the $Er^{3+}-Yb^{3+}$ codoped TiO_2 samples not only plays the role of disperser but it is also a sensitizer for the Er^{3+} ion. This dual effect leads to larger PL intensity in the $Er^{3+}-Yb^{3+}$ codoped TiO_2 system than in the $Er^{3+}-Y^{3+}$ codoped TiO_2 system. However, when the concentration of Yb^{3+} ions reaches 50 mol %, the back energy transfer effect from Er^{3+} to Yb^{3+} will deteriorate the ~1.54 μm PL efficiency.

ACKNOWLEDGMENTS

This work was financially supported by the National Science Council of the Republic of China, Taiwan, under Contract Nos. NSC90-2216-E-009-041 and NSC90-2216-E-213-001.

[1] M. J. Weber, J. Non-Cryst. Solids **123**, 208 (1990).
[2] W. F. Krupke and J. B. Gruber, J. Chem. Phys. **39**, 1024 (1963).
[3] W. F. Krupke and J. B. Gruber, J. Chem. Phys. **41**, 1225 (1964).
[4] O. Lumholt, T. Rasmissen, and A. Bjarklev, Electron. Lett. **29**, 495 (1993).
[5] P. Blixt, J. Nilsson, T. Carlnäs, and B. Jaskorzynska, IEEE Photonics Technol. Lett. **3**, 996 (1991).
[6] K. Arai, H. Namikawa, K. Kumata, T. Honda, Y. Ishii, and T. Handa, J. Appl. Phys. **59**, 3430 (1986).
[7] C. K. Ryu, H. Choi, and K. Kim, Appl. Phys. Lett. **66**, 2496 (1995).
[8] A. F. Obaton, C. Labbé, P. L. Boulanger, B. Elouadi, and G. Boulon, Spectrochim. Acta, Part A **55**, 263 (1999).
[9] C. Urlacher and J. Mugnier, J. Raman Spectrosc. **27**, 785 (1996).
[10] A. Bahtat, M. Bouazaoui, M. Bahtat, and J. Mugnier, Opt. Commun. **111**, 55 (1994).
[11] A. Bahtat, M. Bouderbala, M. Bahtat, M. Bouazaoui, J. Mugnier, and M. Druetta, Thin Solid Films **323**, 59 (1998).
[12] C. C. Ting, S. Y. Chen, W.-F. Hsieh, and H.-Y. Lee, J. Appl. Phys. **90**, 5564 (2001).
[13] C. C. Robinson and J. T. Fournier, J. Phys. Chem. Solids **31**, 895 (1970).
[14] E. Cantelar and F. Cussó, Appl. Phys. B: Lasers Opt. **B69**, 29 (1999).
[15] G. Gu, P. P. Ong, J. Cai, W. Yang, Y. Du, and S. Yang, Thin Solid Films **340**, 230 (1999).
[16] R. D. Shannon and C. T. Prewitt, Acta Crystallogr., Sect. B: Struct. Crystallogr. Cryst. Chem. **B25**, 925 (1969).
[17] H. Ennen, J. Schneider, G. Pomrenke, and A. Axmann, Appl. Phys. Lett. **43**, 943 (1983).
[18] H. Ennen, G. Pomrenke, A. Axmann, K. Eisele, W. Haydl, and J. Schneider, Appl. Phys. Lett. **46**, 381 (1985).
[19] B. E. Warren, *X-ray Diffraction* (Dover, New York, 1990), p. 253.
[20] M. A. Subramanian, G. Aravamudan, and G. V. Subba Rao, Prog. Solid State Chem. **15**, 55 (1983).
[21] C. C. Robinson, J. Non-Cryst. Solids **15**, 11 (1974).

[22] S. Y. Chen, C. C. Ting, and C. H. Li, J. Mater. Chem. **12**, 1118 (2002).
[23] K. Sun, W. H. Lee, and W. M. Risen, Jr., J. Non-Cryst. Solids **92**, 145 (1987).
[24] R. F. Bartholomew, B. L. Butler, H. L. Hoover, and C. K. Wa, J. Am. Ceram. Soc. **63**, 481 (1980).
[25] A. A. Salem, R. Kellner, and M. Grasserbauer, Glass Technol. **35**, 135 (1994).
[26] B. A. Block and B. W. Wessels, Appl. Phys. Lett. **65**, 25 (1994).
[27] B. R. Judd, Phys. Rev. **127**, 750 (1962).
[28] R. M. Moon, W. C. Koehler, H. R. Child, and L. J. Raubenheimer, Phys. Rev. **176**, 722 (1968).
[29] E. F. Artemev, Sov. J. Quantum Electron. **11**, 1266 (1981).
[30] E. Maurice, G. Monnom, B. Dussardier, and D. B. Ostrowsky, J. Opt. Soc. Am. B **13**, 693 (1996).
[31] L. Jackel, A. Y. Yan, E. M. Vagel, A. V. Lehmen, J. J. Johnson, and E. Snitzer, Appl. Opt. **31**, 3390 (1992).